Plasmon-phonon coupling in large-area graphene dot and antidot arrays fabricated by nanosphere lithography

Xiaolong Zhu,[†,‡] Weihua Wang,[†,‡] Wei Yan,[†,‡] Martin B. Larsen,[‡,¶] Peter Bøggild,[‡,¶] Thomas Garm Pedersen,[‡,§] Sanshui Xiao,[*,†,‡] Jian Zi,[‖] and N. Asger Mortensen[*,†,‡]

Department of Photonics Engineering, Technical University of Denmark, DK-2800 Kongens Lyngby, Denmark, Center for Nanostructured Graphene (CNG), Technical University of Denmark, DK-2800 Kongens Lyngby, Denmark, Department of Micro and Nanotechnology, DK-2800 Kongens Lyngby, Denmark, Department of Physics and Nanotechnology, Aalborg University, DK-9220 Aalborg, Denmark, and Department of Physics, Key Laboratory of Micro- and Nano-Photonic Structures (Ministry of Education) and State Key Laboratory of Surface Physics, Fudan University, Shanghai 200433, China

E-mail: saxi@fotonik.dtu.dk; asger@mailaps.org

[*]To whom correspondence should be addressed
[†]DTU Fotonik
[‡]CNG
[¶]DTU Nanotech
[§]Aalborg University
[‖]Fudan University

Experimental Section

Monolayer graphene films grown by chemical vapor deposition (CVD) were wet transferred onto the Si/SiO_2 substrate. In the first step, a 150 nm poly(methylmethacrylate)(PMMA) film was spin-coated onto the graphene covered copper foil and dried at 170^oC for 10 min. Subsequently, a PMMA/graphene membrane was obtained by etching away the copper foil in a $Fe(NO_3)_3/H_2O$ solution and then transferred. Finally, we dissolved the PMMA in acetone and cleaned the graphene surface afterwards. The oxygen plasma etching process was performed by using ICP-DRIE (manufactured by STS) plasma etching system with a power of 800 W and base pressure of 94 mTorr. Pure oxygen gas was used as plasma source. We measured the reflected light intensities in Figure 4b using a Fourier transform infrared spectrometer (Bruker V70v) coupled to an infrared microscope (with a 15X objective) under ambient conditions. The detector is cooled by liquid nitrogen. The other spectra are measured under oblique incidence by using a reflection unit in the macro optical path of Bruker V80v, within a vacuum environment.

Quality of graphene nanostructures

In order to demonstrate the quality of graphene nanostructures, we do the fast Flourier transformation (FFT) according to the patterns of graphene dots and antidots arrays, as shown in Fig. 1a and 1b. The corresponding FFTs (Fig1. c and d) show the six bright first-order peaks associated with the hexagonal structures. The high order peaks further confirmend that the graphene structures are arranged regularly in a hexagonal lattice. Corresponding density distributions are also shown to demonstrate the uniformity of the graphene nanostructures.

The effect of disorder and lack of circular shapes will influence the resonance frequencies at some extent. Indeed, the size vibration of the spheres templates (1% in our case) and the fabrication of graphene structures by oxygen plasma etching can impart atomic-scale defects. However, these disorders (with 1-2%) mainly influence the plasmon peak width in the graphene structures, and have less effect in plasmon peak position. For the effect of the lack of circular shapes, we have

done a few finite element calculations on graphene structures, varying the structures from disk, ellipse to hexagon. It is easy to find that both the plasmonic spectra and field pattern change a little. For example, from a disk to a hexagon (Fig. 2), the plasmon frequency difference is only (0.159 -0.151) / 0.151 = 5%, which is acceptable comparing to our experimental accuracy. In order to distinguish the resonance frequencies well, we use a relatively small loss, an intrinsic relaxation time of 2450 fs, in the numerical calculations.

Description of the graphene conductivity

In the numerical simulations, the surface conductivity of graphene is considered in the zero-parallel wave vector limit of the random-phase approximation (local RPA), including the effect of finite temperature ($T = 300\,\mathrm{K}$), as follows[1]

$$\sigma(\omega) = \frac{2e^2 k_B T}{\pi\hbar^2}\frac{i}{\omega + i\tau^{-1}}\ln\left[2\cosh\left(E_F/2k_BT\right)\right] + \frac{e^2}{4\hbar}\left[H(\omega/2) + \frac{4i\omega}{\pi}\int_0^\infty d\varepsilon \frac{H(\varepsilon) - H(\omega/2)}{\omega^2 - 4\varepsilon^2}\right] \tag{1}$$

where

$$H(\varepsilon) = \frac{\sinh\left(\hbar\varepsilon/k_BT\right)}{\cosh\left(E_F/k_BT\right) + \cosh\left(\hbar\varepsilon/k_BT\right)} \tag{2}$$

and an intrinsic relaxation time $\tau = \mu E_F/ev_F^2$ at room temperature is used. Here, E_F is the Fermi level, v_F is the Fermi velocity, and μ is the dc mobility. The as-transferred CVD-graphene is hole-doped with a Fermi level of approximately -0.35 eV as in our previous work.[2] After the O_2 plasma etching, the Fermi level decreases to -0.45 eV, considering the promoted charge doping by oxygen atoms or ions binding with the carbon dangling bonds. By exposing the samples to nitric acid vapor for 5 min, the Fermi level could further decrease, see Figure S1. The used dc mobility in our simulations is , which is good to obtain the resonant features and reasonable for CVD-graphene.[3]

Plasmon-phonon coupling in graphene

When graphene is deposited on a polar substrate (such as SiO_2 used in our experiments), the electronic properties will be greatly modified by the surface optical phonon scattering via the Fröhlich interaction,[4–10] and thereby the electronic excitations differ from graphene on a nonpolar substrate. In the theoretical studies of the effects of surface phonons, the polar substrates are described by a frequency dependent dielectric function, which can be written as[4]

$$\varepsilon(\omega) = \varepsilon_h + \sum_i f_i \frac{{\omega_{\mathrm{TO}}^{(i)}}^2}{{\omega_{\mathrm{TO}}^{(i)}}^2 - \omega^2 - i\omega\tau^{-1}} \tag{3}$$

where ε_h is the dielectric constant at high frequency, $\omega_{\mathrm{TO}}^{(i)}$ denotes the ith transverse optical phonon mode frequency, and f_i is the corresponding mode strength. f_i satisfies the sum rule $\sum_i f_i = \varepsilon_l - \varepsilon_h$, where ε_l is the low-frequency dielectric constant. Neglecting the dielectric response of a thin graphene layer and the imaginary part of the substrate response, the frequencies $\omega_{\mathrm{S}}^{(i)}$ of the surface phonons are determined by $\varepsilon(\omega) + 1 = 0$. In SiO_2, there are two surface phonon modes contributing to the plasmon phonon coupling in the frequency region considered, and after some straightforward algebra we arrive at

$$\begin{aligned}{\omega_{\mathrm{TO}}^{(1)}}^2 = {} & \frac{(\varepsilon_h+1)(\varepsilon_l+1)\left({\omega_{\mathrm{S}}^{(1)}}^2 + {\omega_{\mathrm{S}}^{(2)}}^2\right)}{2\left(\varepsilon_h+1+f_1\right)(\varepsilon_l+1)} \\ & + \frac{\sqrt{(\varepsilon_h+1)^2(\varepsilon_l+1)^2\left({\omega_{\mathrm{S}}^{(1)}}^2 + {\omega_{\mathrm{S}}^{(2)}}^2\right)^2 - 4(\varepsilon_h+1+f_1)(\varepsilon_h+1+f_2)(\varepsilon_h+1)(\varepsilon_l+1){\omega_{\mathrm{S}}^{(1)}}^2{\omega_{\mathrm{S}}^{(2)}}^2}}{2\left(\varepsilon_h+1+f_1\right)(\varepsilon_l+1)}\end{aligned} \tag{4a}$$

$$\omega_{\mathrm{TO}}^{(2)^2} = \frac{(\varepsilon_h+1)(\varepsilon_l+1)\left(\omega_{\mathrm{S}}^{(1)^2}+\omega_{\mathrm{S}}^{(2)^2}\right)}{2\left(\varepsilon_h+1+f_2\right)(\varepsilon_l+1)}$$
$$+\frac{\sqrt{(\varepsilon_h+1)^2(\varepsilon_l+1)^2\left(\omega_{\mathrm{S}}^{(1)^2}+\omega_{\mathrm{S}}^{(2)^2}\right)^2-4(\varepsilon_h+1+f_1)(\varepsilon_h+1+f_2)(\varepsilon_h+1)(\varepsilon_l+1)\omega_{\mathrm{S}}^{(1)^2}\omega_{\mathrm{S}}^{(2)^2}}}{2\left(\varepsilon_h+1+f_2\right)(\varepsilon_l+1)} \tag{4b}$$

Here, TO modes 1 and 2 are found from Eqs. (S3a) and (S3b), respectively. The parameters in Eqs. (S3) can be extracted from the experimental measurements, by applying all the parameters used in the Ref.,[8] and then we get two values for $\omega_{\mathrm{TO}}^{(1)}$ and $\omega_{\mathrm{TO}}^{(2)}$. Now we proceed to calculate the coupled plasmon-phonon mode dispersion by using Eq.(S2) and the optical conductivity $\sigma(q,\omega)$ of graphene obtained from random phase approximation.[3,11,12] When graphene sits on SiO_2 in vacuum, the dispersion of surface modes is defined by[3]

$$\frac{1}{\sqrt{q^2-\omega^2/c^2}}+\frac{\varepsilon(\omega)}{\sqrt{q^2-\varepsilon(\omega)\omega^2/c^2}}=-\frac{i\sigma(q,\omega)}{\omega\varepsilon_0} \tag{5}$$

The only task is to find the mode frequencies ω_q for each wave vector q in Eq. (3), which is easily evaluated numerically. In graphene nanostructures, the plasmon excitations satisfy the quasi-static scaling law[13] and the effective wave vector for dipole plasmon resonances in disks is given by $q=1/R$.[13] Thus Eq. (S3) can be evaluated for different disk radii. Apart from these quasi-static calculations, we also perform full-wave numerical simulations with the standard finite-integration technique (CST microwave studio). By noticing that q

k_F in our experiments, where $k_F=\left|E_F\right|/\hbar v_F$ is the Fermi wave vector, the optical conductivity $\sigma(q,\omega)$ of graphene can be approximated as $\sigma(q\to 0,\omega)$, which is Eq. (S1).

Supplementary figures

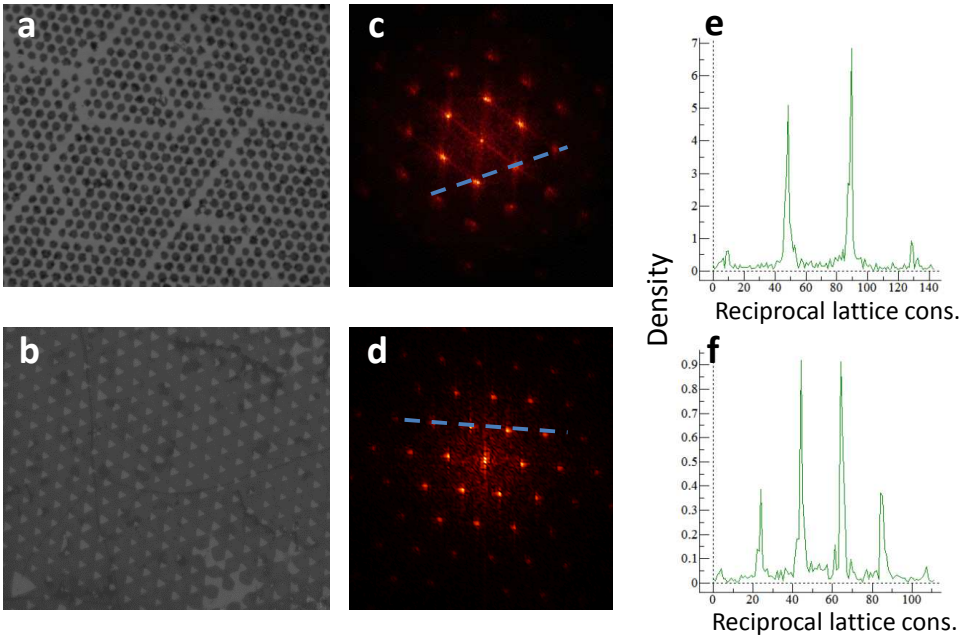

Figure S1: (a-b) Graphene dots and antidots arrays, in real-space SEM images. (c-d) FFT patterns corresponding to a-b. (e-f) Corresponding density vs. the reciprocal lattice constants, labeled by dashed lines.

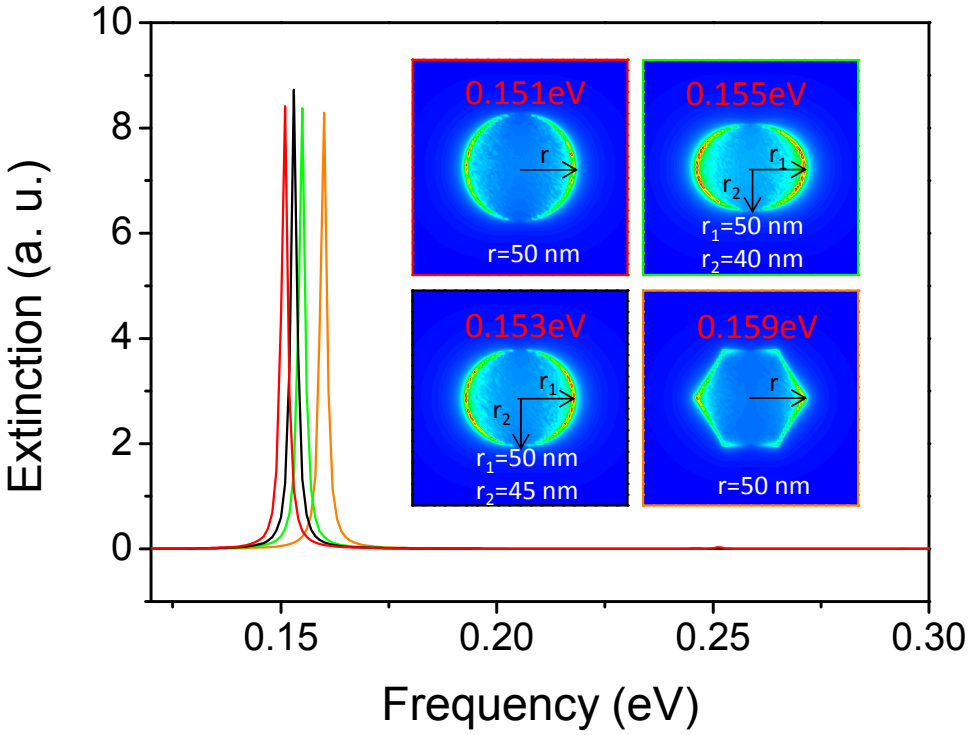

Figure S2: Finite element calculations on isolated graphene elements. Insets are the corresponding field distributions for the elements with different parameters.

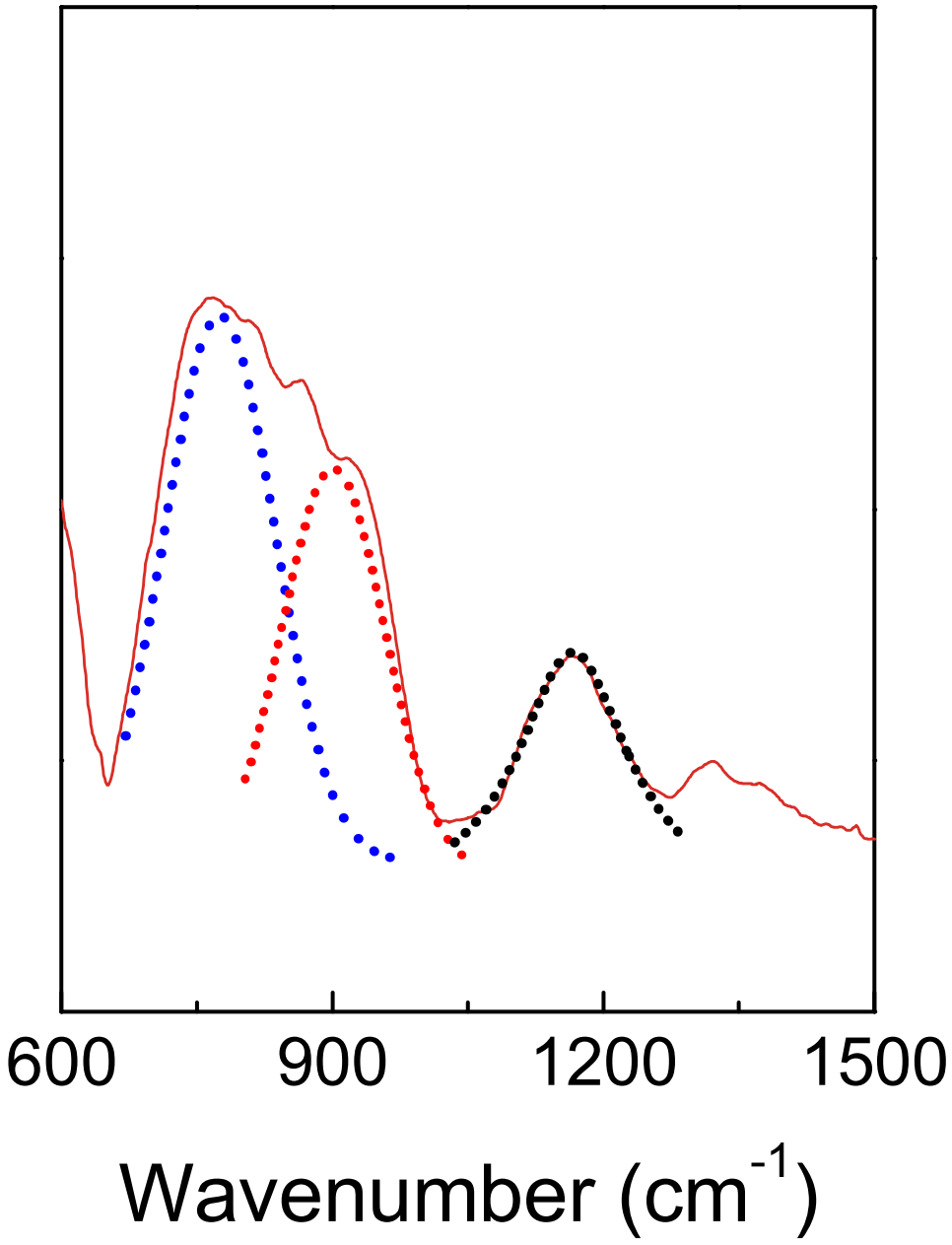

Figure S3: The multi peak analysis for Figure 4b.

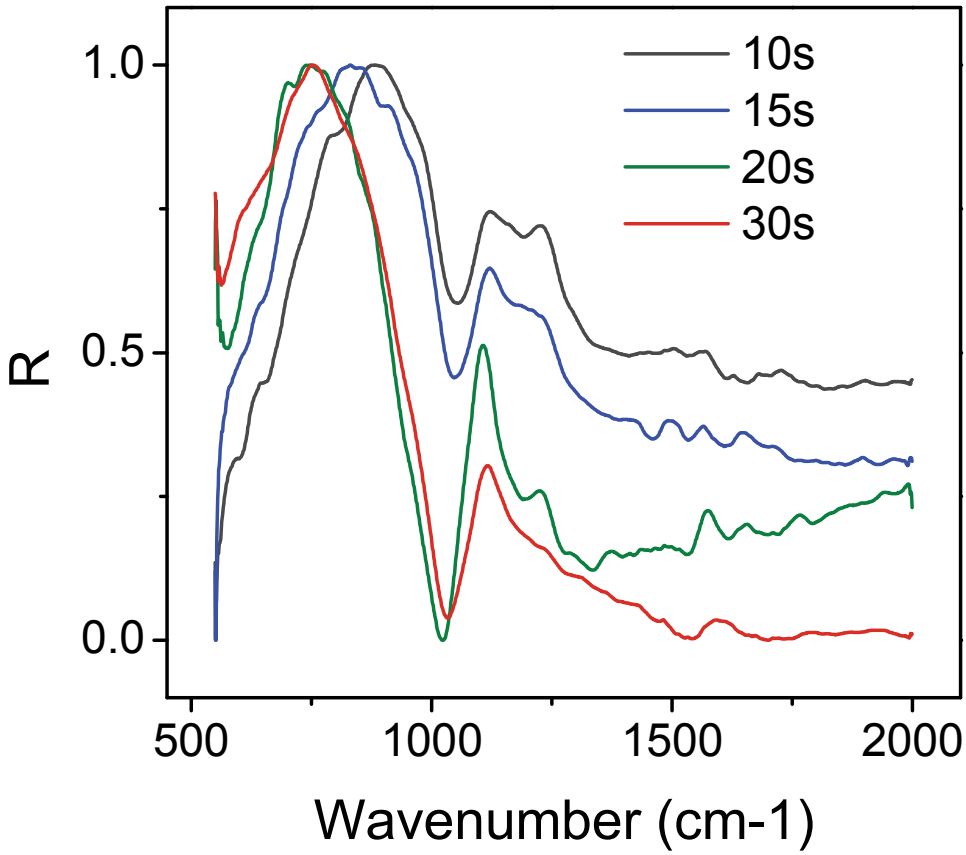

Figure S4: Normalized reflection spectra of the graphene antidot arrays with different time of O_2 plasma etching. From the measurements, we can find that the resonances are sensitive to the geometrical aspect ratio. When the antidot size (etching time) increases, the average electron density will also change. The resonance suffers a redshift and intensity of the resonance increases. The spectra are measured under a set-up consisting of an infrared microscope coupled to a Fourier-transform infrared spectrometer (FTIR).

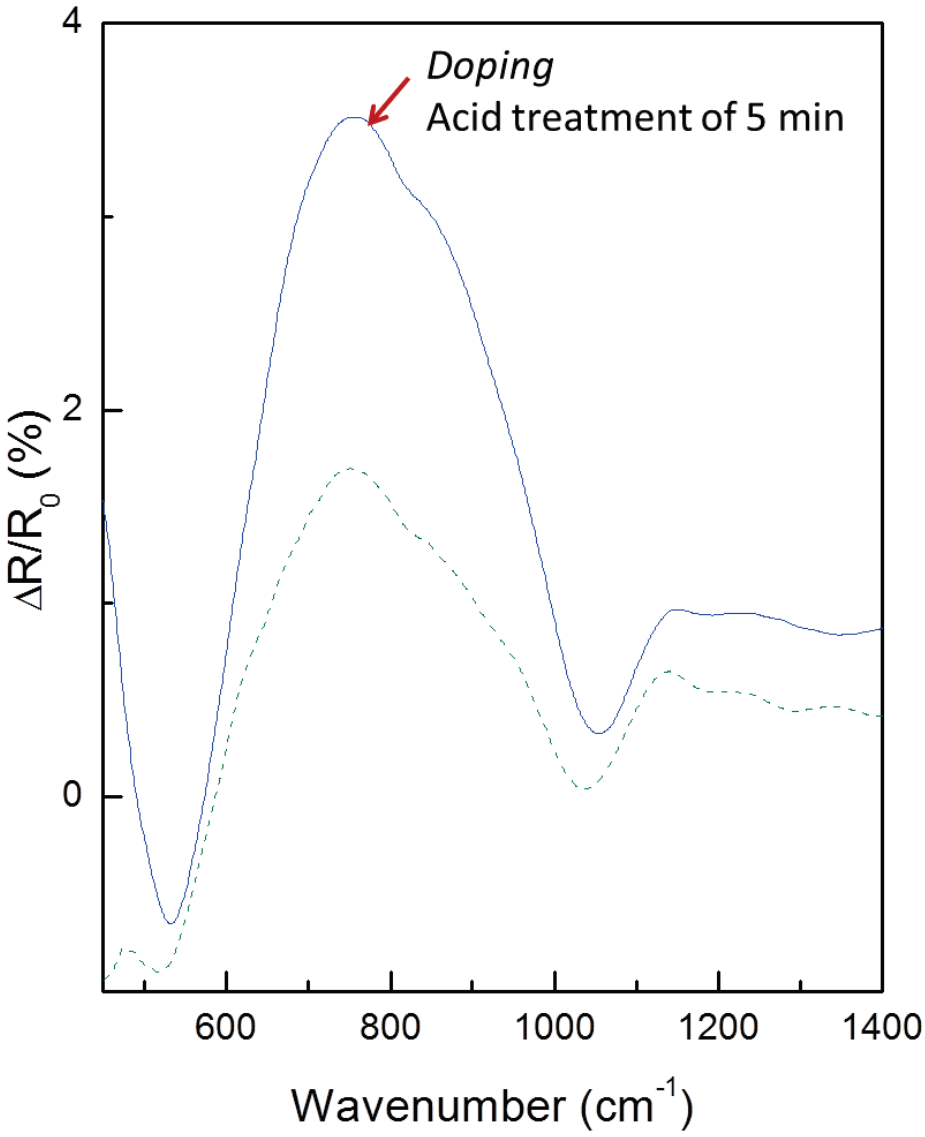

Figure S5: Resonance spectra of graphene dots with $R = 160$ nm on SiO_2 at different doping levels. By exposing the samples to nitric acid vapour for 5 min, the as-prepared graphene could be further doped. As the Fermi level further decreases (for hole doping) and the carrier density increases, the plasmon resonance shifts slightly to higher frequency with doping while the linewidth decreases.

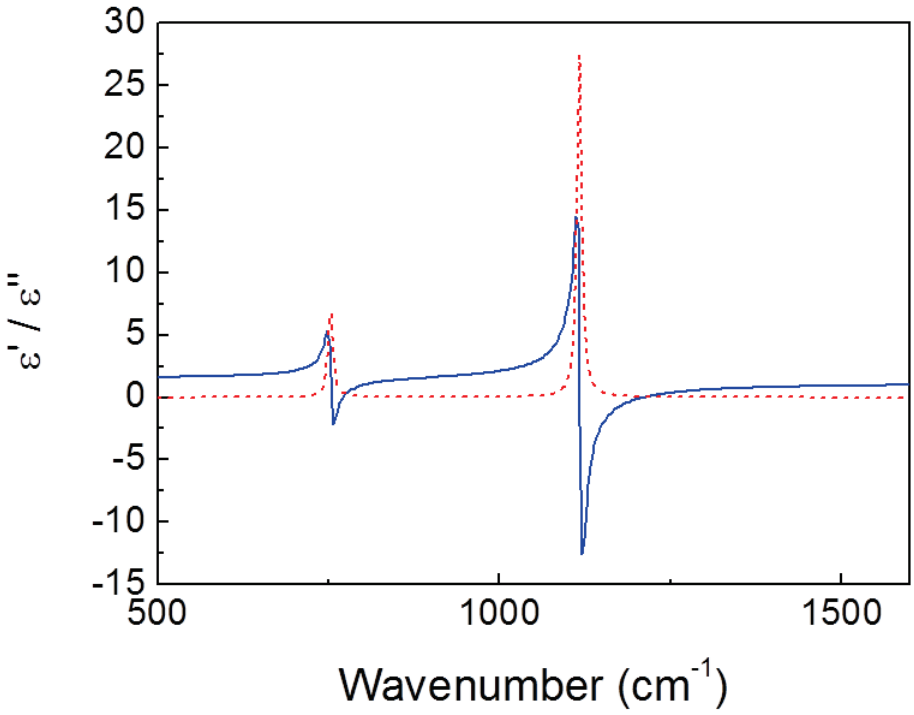

Figure S6: The dielectric permittivity of polar SiO_2 used in the simulations, where ε' and ε'' denote the real (the solid line) and the imaginary (the dashed line) part of the permittivity, respectively.

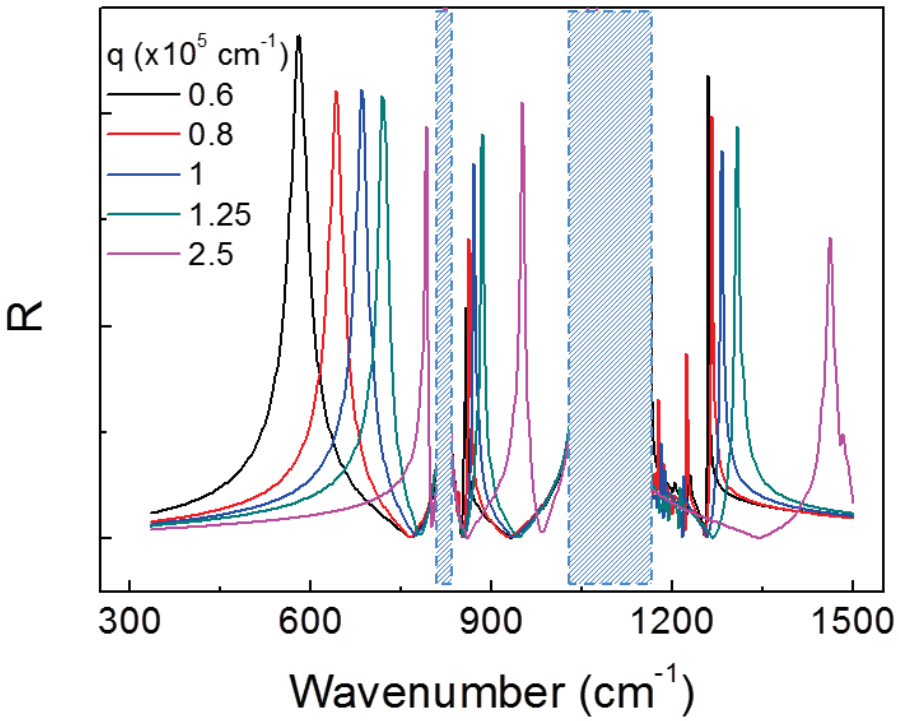

Figure S7: The simulated spectra of graphene dots with different diameters (different q, $q = 1/R$), calculated by solving Maxwell's equations using the local RPA conductivity of graphene and the polar dielectric function of SiO_2. The intrinsic phonon resonances of bare SiO_2 at around 800 and 1100 cm^{-1} are shadowed. It should be noticed that the resonance spectrum with an asymmetric shape resembles the Fano resonances.[14] The physics relies on the interference between the continuum state of the background reflections from SiO_2 substrate, and the discrete state of the graphene plasmon resonance. The continuum state in our structures has a noticeable weight, since the optical phonon resonances of SiO_2 induce a significant electric response to the substrate. This further manifests its role in the apparent asymmetric line shape, i.e., increasing the interference strength.

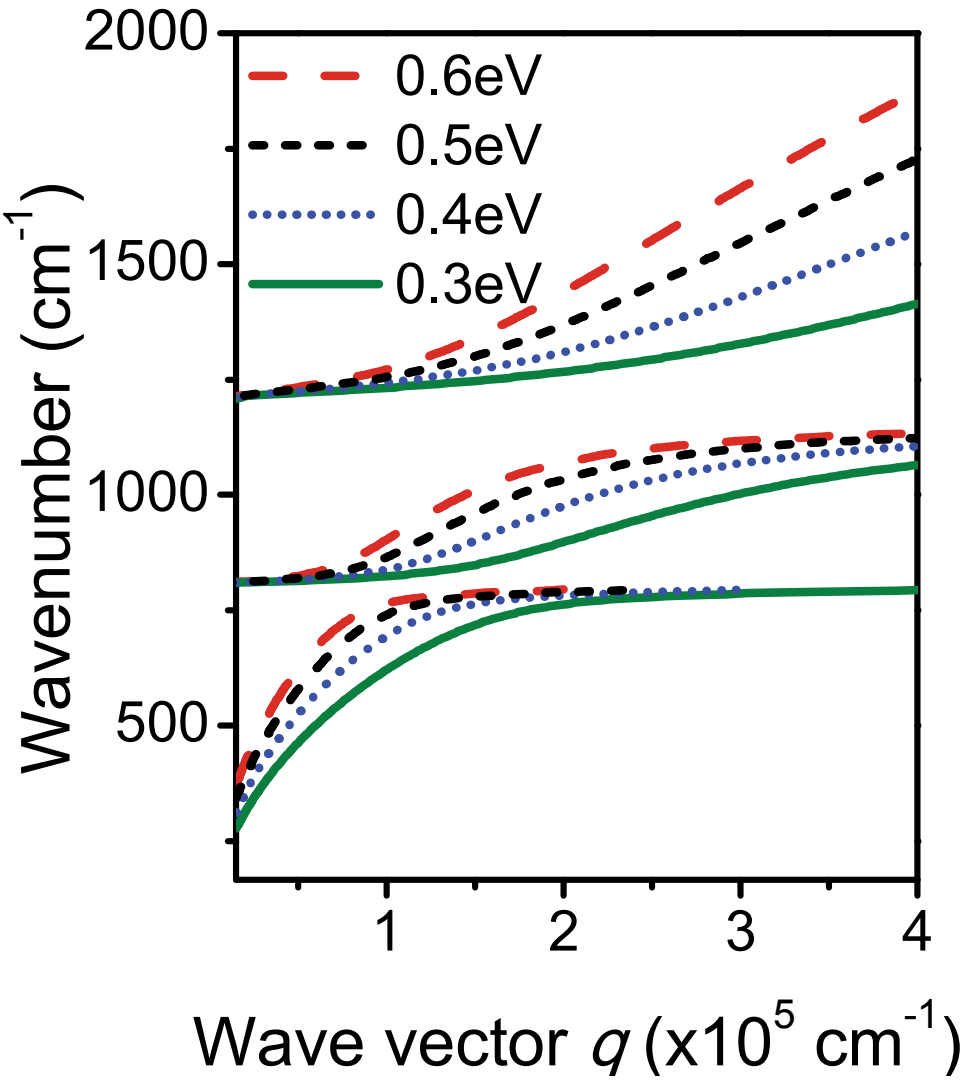

Figure S8: Theoretical calculations of the plasmon-phonon hybridization under different Fermi levels. In order to fit the experimental results, the theoretical calculations of the plasmon-phonon hybridization under different Fermi levels are implemented. By comparing the experimental results and the theoretical calculations, we find that the Fermi level prediction at -0.4 to -0.45 eV is reasonable and matches well with the measurements.

References

(1) Falkovsky, L. A.; Pershoguba, S. S. *Phys. Rev. B* **2007**, *76*, 153410.

(2) Zhu, X.; Yan, W.; Jepsen, P. U.; Hansen, O.; Mortensen, N. A.; Xiao, S. *Appl. Phys. Lett.* **2013**, *102*, 131101.

(3) Jablan, M.; Buljan, H.; Soljačić, M. *Phys. Rev. B* **2009**, *80*, 245435.

(4) Chen, J.-H.; Jang, C.; Xiao, S.; Ishigami, M.; Fuhrer, M. S. *Nat. Nanotechnol.* **2008**, *3*, 206–209.

(5) Fratini, S.; Guinea, F. *Phys. Rev. B* **2008**, *77*, 195415.

(6) Hwang, E. H.; Das Sarma, S. *Phys. Rev. B* **2013**, *87*, 115432.

(7) Lu, J.; Loh, K. P.; Huang, H.; Chen, W.; Wee, A. T. S. *Phys. Rev. B* **2009**, *80*, 113410.

(8) Liu, Y.; Willis, R. F. *Phys. Rev. B* **2010**, *81*, 081406.

(9) Koch, R. J.; Seyller, T.; Schaefer, J. A. *Phys. Rev. B* **2010**, *82*, 201413.

(10) Yan, H.; Low, T.; Zhu, W.; Wu, Y.; Freitag, M.; Li, X.; Guinea, F.; Avouris, P.; Xia, F. *Nat. Photon.* **2013**, *7*, 394–399.

(11) Wunsch, B.; Stauber, T.; Sols, F.; Guinea, F. *New J. Phys.* **2006**, *8*, 318.

(12) Hwang, E. H.; Das Sarma, S. *Phys. Rev. B* **2007**, *75*, 205418.

(13) Wang, W.; Apell, S. P.; Kinaret, J. M. *Phys. Rev. B* **2012**, *86*, 125450.

(14) Miroshnichenko, A. E.; Flach, S.; Kivshar, Y. S. *Rev. Mod. Phys.* **2010**, *82*, 2257–2298.